

FOR OFFICIAL USE ONLY



NAVAL AIR WARFARE CENTER AIRCRAFT DIVISION
PATUXENT RIVER, MARYLAND



TECHNICAL INFORMATION MEMORANDUM

REPORT NO: NAWCADPAX/TIM-2016/216

THERMAL FATIGUE OF INCONEL ALLOY DA718

by

**E. U. Lee
M. Stanley
B. Pregger**

27 October 2016

Approved for public release.

FOR OFFICIAL USE ONLY

DEPARTMENT OF THE NAVY
NAVAL AIR WARFARE CENTER AIRCRAFT DIVISION
PATUXENT RIVER, MARYLAND

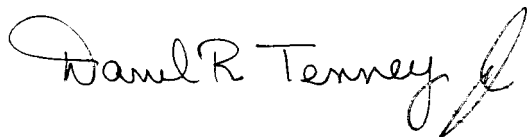
NAWCADPAX/TIM-2016/216
27 October 2016

THERMAL FATIGUE OF INCONEL ALLOY DA718

by

E. U. Lee
M. Stanley
B. Pregger

RELEASED BY:



27 Oct 2016

DARREL R. TENNEY, JR. / AIR-4.4.4 / DATE
Head, Materials Engineering Division
Naval Air Warfare Center Aircraft Division

FOR OFFICIAL USE ONLY

| REPORT DOCUMENTATION PAGE | | | | Form Approved OMB No. 0704-0188 | |
|---|--------------|--|-------------------------------|--|--|
| Public reporting burden for this collection of information is estimated to average 1 hour per response, including the time for reviewing instructions, searching existing data sources, gathering and maintaining the data needed, and completing and reviewing this collection of information. Send comments regarding this burden estimate or any other aspect of this collection of information, including suggestions for reducing this burden, to Department of Defense, Washington Headquarters Services, Directorate for Information Operations and Reports (0704-0188), 1215 Jefferson Davis Highway, Suite 1204, Arlington, VA 22202-4302. Respondents should be aware that notwithstanding any other provision of law, no person shall be subject to any penalty for failing to comply with a collection of information if it does not display a currently valid OMB control number. PLEASE DO NOT RETURN YOUR FORM TO THE ABOVE ADDRESS. | | | | | |
| 1. REPORT DATE 27 October 2016 | | 2. REPORT TYPE Technical Information Memorandum | | 3. DATES COVERED | |
| 4. TITLE AND SUBTITLE Thermal Fatigue of Inconel Allow DA718 | | | | 5a. CONTRACT NUMBER | |
| | | | | 5b. GRANT NUMBER | |
| | | | | 5c. PROGRAM ELEMENT NUMBER | |
| 6. AUTHOR(S) E. U. Lee M. Stanley B. Pregger | | | | 5d. PROJECT NUMBER | |
| | | | | 5e. TASK NUMBER | |
| | | | | 5f. WORK UNIT NUMBER | |
| 7. PERFORMING ORGANIZATION NAME(S) AND ADDRESS(ES) Naval Air Warfare Center Aircraft Division Bldg. 2188, Code 4.3.4 48066 Shaw Road Patuxent River, MD 20670 | | | | 8. PERFORMING ORGANIZATION REPORT NUMBER NAWCADPAX/TIM-2016.216 | |
| 9. SPONSORING/MONITORING AGENCY NAME(S) AND ADDRESS(ES) Office of Naval Research 875 N. Randolph Street, Room 1143B Arlington, VA 22203 | | | | 10. SPONSOR/MONITOR'S ACRONYM(S) | |
| | | | | 11. SPONSOR/MONITOR'S REPORT NUMBER(S) | |
| 12. DISTRIBUTION/AVAILABILITY STATEMENT Approved for public release. | | | | | |
| 13. SUPPLEMENTARY NOTES | | | | | |
| 14. ABSTRACT The thermal fatigue behavior of an Inconel alloy DA718 was studied to clarify the induced axial stress, diametral strain, and change in microstructure and fractograph under thermal fatigue cycling between the predetermined maximum and minimum temperatures in air. The minimum axial stress became less compressive with increasing number of thermal fatigue cycle and temperature. The diametral strain was constant in the initial stage of thermal fatigue cycling but decreased later. The decrease occurred earlier at higher temperatures and during longer holding time. The intragrain precipitates γ' and γ'' were grown, and γ'' particle-depleted zones were formed near grain boundaries due to γ'' to δ phase transformation during the thermal fatigue cycling. This microstructure change resulted in the variation of axial stress and diametral strain, intergranular cracking, and eventual thermal fatigue failure. | | | | | |
| 15. SUBJECT TERMS Thermal Fatigue, Inconel Allow DA718 | | | | | |
| 16. SECURITY CLASSIFICATION OF: | | | 17. LIMITATION OF ABSTRACT | 18. NUMBER OF PAGES | 19a. NAME OF RESPONSIBLE PERSON E. U. Lee |
| a. REPORT | b. ABSTRACT | c. THIS PAGE | | | 19b. TELEPHONE NUMBER (include area code) |
| Unclassified | Unclassified | Unclassified | SAR | | |

Standard Form 298 (Rev. 8-98)
Prescribed by ANSI Std. Z39-18

SUMMARY

An Inconel alloy DA718 specimens were subjected to thermal fatigue cycling between the predetermined maximum temperature T_{\max} and the minimum temperature T_{\min} , or with addition of holding at the both temperatures. The T_{\max} ranged from 1200 to 1550°F, and the T_{\min} was 600°F. During the thermal fatigue cycling, the specimen was constrained to prevent any longitudinal expansion or shrinkage in a MTS machine. The induced axial stress, diametral strain, and specimen temperature were continuously measured. The test results indicated that

- The thermally induced minimum axial stress became less compressive with increasing thermal cycle, higher T_{\max} , and longer holding period.
- The diametral strain at the specimen mid-length changed cyclically during thermal fatigue cycling. The maximum was constant initially and decreased later. This was noticed earlier for higher temperature and longer holding time.
- During the thermal fatigue cycling, intragrain γ' and γ'' precipitates were coarsened, γ'' transformed to δ phase, and γ'' -depleted zones were formed near grain boundaries. Those zones were prone to intergranular cracking.

Contents

| | <u>Page No.</u> |
|---|-----------------|
| Introduction..... | 1 |
| Background | 1 |
| Purpose..... | 1 |
| Methods..... | 1 |
| Material | 1 |
| Specimen | 2 |
| Test Apparatus | 2 |
| Thermal Fatigue Cycling | 3 |
| Micrography and Fractography..... | 3 |
| Experimental Results | 3 |
| Variation of Axial Stress during Simple Thermal Cycling..... | 3 |
| Variation of Diametral Strain during Simple Thermal Cycling..... | 4 |
| Variation of Axial Stress during Thermal and Holding Cycle | 4 |
| Variation of Diametral Strain during Thermal and Holding Cycle | 4 |
| Comparison of Minimum Axial Stresses for Simple Thermal Cycling and | 4 |
| Thermal and Holding Cycling | |
| Micrography..... | 4 |
| Fractography | 5 |
| Discussion | 5 |
| Stress and Strain under Thermal Fatigue Cycling | 5 |
| Variation of Axial Stress and Diametral Strain during Thermal | 6 |
| Fatigue Cycling | |
| Comparison of Minimum Axial Stresses for Simple Thermal Cycling..... | 7 |
| and Thermal and Holding Cycling | |
| Microstructural Change during Thermal Fatigue Cycling..... | 7 |
| Conclusions..... | 9 |
| Recommendation | 10 |
| References..... | 11 |
| Appendices | |
| A. List of Figures | 13 |
| B. Tables | 21 |
| Distribution | 23 |

ACKNOWLEDGEMENTS

The support from the NISE Research Program is gratefully acknowledged. Furthermore, the authors appreciate the NAE Chief Technology Officer, Dr. James B. Sheehy, the Associate Director of Research Programs, NAE Chief Technology Office, Ms. Kristi Wiegman, and the Lead Air Vehicle Engineering Technologist, Mr. Jerry Rubinsky for their guidance and interest.

INTRODUCTION

BACKGROUND

Structural components experience various operating conditions, often involving complex combination of cyclic temperature, cyclic mechanical stress, and varying environments. Especially, some of them are subjected to a variety of thermal and thermomechanical loads. If the stresses in a component develop under thermal cycling without external loading, the term thermal fatigue or thermal stress fatigue is used. On the other hand, thermal fatigue can also develop even under conditions of uniform temperature, caused by internal constraints such as different grain orientations or anisotropy of the thermal expansion coefficient of different metallurgical constituents. Internal stress and strain can be of sufficiently high magnitude to cause distortion, cracking and/or surface irregularities in the material. Consequently, thermal cycling results in damage and deterioration of the microstructure. By following the changes in microstructure, and by observing the changes in distribution of important microconstituents with increasing thermal damage, it would be possible to gain some knowledge of the mechanism of thermal fatigue.

Though thermal fatigue failures are by no means a new problem, the trends in modern technology to higher temperatures and cyclic operations have increased their occurrence and damaging effects. Many examples have been discussed in the literature, for example, aircraft engines, power generating plants, petroleum refineries, and nuclear reactors. Considering the importance, there is little fundamental information available on thermal fatigue of ductile materials.

PURPOSE

The purpose of this study is to clarify the effects of the temperature and number of thermal fatigue cycle, and the concurrent microstructural change on the thermal fatigue behavior of a ductile material, and establish its controlling mechanism.

METHODS

MATERIAL

A commercial Inconel alloy 718 is a precipitation hardenable alloy designed to have high yield, tensile and creep-rupture properties. There are three versions of wrought Inconel alloy 718 used in the production of gas turbine engine components (reference 1). "Standard Processed" alloy 718 is used for noncritical or difficult to make shapes and has an average grain size of ASTM 4-6. "High Strength Processed" alloy 718 is used for more highly stressed components with less complex configurations and has an average grain size of ASTM 8. The third version, "Direct Age Processed" alloy 718 or DA718 achieves the highest tensile at a further expense in shape making capability. This material has an average grain size of ASTM 10, and used in disc application where high tensile and fatigue strength are required. The DA718 shows significant improvements in tensile strength and low cycle fatigue properties, but exhibits low stress rupture

life in the low stress-high temperature regime. For compressor and turbine disc application, this material meets the required improvement and offers a low cost alternative to powder metallurgy Rene'95. However, its thermal fatigue resistance remains to be fully clarified.

Its nominal chemical composition is shown in Table B-1. In the fully heat treated condition, DA718 consists of a γ matrix, γ' , γ'' , δ precipitate phases, and small amounts of NbC carbides and TiN nitrides. The major strengthening precipitate in DA718 is the Ni_3Nb γ'' phase, which is coherent and has a DO_{22} crystal structure (reference 2). This precipitate is disc-shaped and has a diameter of 20-40 μm after conventional aging treatments. The γ'' strengthening is due to coherency strains that arise during precipitation. A smaller amount of $\text{Ni}_3(\text{Al,Ti})$ γ' phase (L1_2 structure) is present in the alloy, and this precipitate forms as a spherical shaped particle. The γ'' phase begins to solution between 1550 and 1600°F, while the solvus of the γ' phase is somewhat lower. Both the γ' and γ'' phases are metastable, whereas the stable phase is Ni_3Nb δ , which is incoherent and has an orthorhombic crystal structure. This phase forms as intragranular laths along $\{111\}$, or at grain boundaries. Precipitation of the δ phase is usually more pronounced in the 1700-1750°F range, and the solvus is typically near 1800°F. The δ phase plays an important role in the control of grain size, since its presence can inhibit grain coarsening during processing and heat treatment. In this study, the DA718 was chosen as the specimen material, and its scanning electron micrograph is shown in Figure A-1. This figure indicates δ phase plates along grain boundaries and within grains, and tiny intragrain γ' and γ'' precipitates in γ matrix.

SPECIMEN

The employment of an hourglass specimen in thermal fatigue tests would be of vital benefit in improving the geometry stability. A uniform longitudinal temperature distribution is not required; it is only necessary that the maximum temperature occurs in the minimum cross section. The use of induction heating can produce a uniform radial temperature. Only the diametral strain and temperature need to be recorded as a function of thermal load in order to compute the actual strain range in the minimum cross section. Therefore, the hourglass specimen was selected as the test specimen in this study.

Hourglass specimens were machined from a 1.5 in. diameter round bar of DA718 in L-orientation. The length was 6 in., the minimum diameter 0.25 in., the blending fillet radius 2.25 in., and the grip section diameter 0.5 in.

TEST APPARATUS

The thermal fatigue testing apparatus consists of an induction heating coil, a tubular ring diffuser of compressed air with several holes, both of which surround a specimen, and a diametral extensometer at the specimen mid-length in a MTS machine, Figure A-2.

Its essential feature is the imposition of a complete longitudinal constraint on the test specimen with a couple of locked hydraulic grips in a MTS machine. To develop a cyclic thermal stress in the test specimen, the specimen temperature is cycled by programmed induction heating and

compressed-air cooling. A solenoid-operated valve is used to supply compressed-air to the tubular ring diffuser during the cooling phase of the cycle.

The longitudinal or axial load or stress, induced by the expansion and contraction of the specimen during thermal cycling, is measured by a load-cell above the specimen. The specimen temperature during the testing is measured with a chromel-alumel thermocouple, spot-welded to the mid-length of the specimen. The thermal strain, induced by the expansion and contraction of the specimen, is measured with a diametral extensometer at the mid-length.

THERMAL FATIGUE CYCLING

The specimen temperature was cycled between the predetermined maximum temperature of the cycle T_{\max} and the minimum temperature of the cycle T_{\min} , or with addition of holding at the both temperatures. The former was defined as Simple Thermal Cycling, and the latter as Thermal and Holding Cycling in this study. The Simple Thermal Cycling was broken down into two components: (1) heat and (2) cool. The Thermal and Holding Cycling was broken down into four components: (1) heat, (2) hold at T_{\max} , (3) cool, and (4) hold at T_{\min} . The T_{\max} ranged from 1200 to 1550°F, and the T_{\min} was 600°F. The time required for each component was longer for higher T_{\max} , taking account of the longer time of induction heating and compressed air cooling. The schemes of the thermal fatigue cycling are shown in Figures A-3(a) and (b), respectively.

During the thermal fatigue cycling, the changing axial (or longitudinal) load in the specimen was measured with a load-cell in the MTS machine continuously. The minimum diameter of the specimen at the mid-length was measured with an extensometer continuously. The measured axial load and diameter of the specimen were converted to the axial stress and diametral strain, and saved in the attached computer.

MICROGRAPHY AND FRACTOGRAPHY

The microstructure of the polished and etched specimen cross-section and the morphology of the specimen fracture surface were examined with a JEOL JSM-6460LV scanning electron microscope, operated at an accelerating voltage of 20 kV.

EXPERIMENTAL RESULTS

VARIATION OF AXIAL STRESS DURING SIMPLE THERMAL CYCLING

The axial or longitudinal stress, induced by thermal cycling, was found to be compressive and changing cyclically. The minimum axial stress of each thermal cycle increased with the increasing number of thermal cycle and increasing maximum temperature, as shown in Figure A-4. In other words, the thermally induced stress became less compressive with increasing number of thermal cycle and increasing maximum temperature applied.

VARIATION OF DIAMETRAL STRAIN DURING SIMPLE THERMAL CYCLING

During the thermal fatigue cycling, the specimen was bulged cyclically at the heated center of the constrained specimen, because of compressive yielding and creep. Correspondingly, the diametral strain changed cyclically. The maximum diametral strain at the mid-length was around 0.01 in./in. and changed little during the thermal cycling for the maximum temperatures below 1400°F, but it decreased with increasing number of thermal cycle at and above 1400°F, as shown in Figure A-5. The decrease in the maximum diametral strain was greater and occurred earlier for the higher maximum temperature of the thermal cycle.

VARIATION OF AXIAL STRESS DURING THERMAL AND HOLDING CYCLE

The features of the minimum axial stress variation during thermal and holding cycling are similar to those for the simple thermal cycling, except the lower minimum axial stress or less compression, as shown in Figure A-6.

VARIATION OF DIAMETRAL STRAIN DURING THERMAL AND HOLDING CYCLE

During the thermal and holding cycling, the maximum diametral strain was about 0.01 in./in. for an initial period and began to decrease at or above 1300°F of the maximum cycle temperature. In the case of maximum cycle temperature 1300°F, the period was 200 cycles, but it was shorter for higher maximum cycle temperatures. On the other hand, for the maximum cycle temperature 1200°F, the maximum diametral strain was 0.0028 in./in. up to 155 cycles and then gradually decreased. Those variations of the maximum diametral strain with number of thermal and holding cycle are shown in Figure A-7.

COMPARISON OF MINIMUM AXIAL STRESSES FOR SIMPLE THERMAL CYCLING AND THERMAL AND HOLDING CYCLING

The minimum axial stresses $(\sigma_z)_{\min}$ for the simple thermal cycling and the thermal and holding cycling are compared in Figure A-8. At the five different maximum cycle temperatures T_{\max} , 1200, 1300, 1350, 1400, and 1550°F, and throughout the applied numbers of thermal cycle, the minimum axial stress is less compressive for the thermal and holding cycling than for the simple thermal cycling.

MICROGRAPHY

The microstructures of the specimens, subjected to simple thermal cycling and thermal and holding cycling, are shown in Figures A-9 and A-10, respectively. Figure A-9(a) depicts an intergranular fracture of a specimen, which was undergone to simple thermal cycling of 600-1350°F. In Figure A-9(b), it is noticeable that γ'' precipitates were depleted and cracks appeared in the zones along grain boundaries during the simple thermal cycling of 600-1400°F. In Figure A-10, it is observable that the initially equi-axed grains (Figure A-1) were elongated and bowed,

and the intragrain and intergranular δ phase rods were bent or bowed during the thermal and holding cycling of 600-1500°F.

FRACTOGRAPHY

Typical SEM fractographs for the specimens, subjected to simple thermal cycling and thermal and holding cycling, are shown in Figures A-11 and A-12, respectively. They indicate:

- A crack was initiated on the specimen surface, and grew inward, creating a slow crack growth area and an overload fracture area.
- The slow crack growth area has beach-marks, containing fatigue-facets with striations, secondary cracks along some striations and cracks along some facet-boundaries.
- In the overload fracture area, equi-axed dimples are noticeable. Near the boundary between the slow crack growth area and overload fracture area, a mixture of dimples and fatigue facets with striations is seen.
- The fractographic features are similar to those for the mechanical fatigue at room temperature.

DISCUSSION

STRESS AND STRAIN UNDER THERMAL FATIGUE CYCLING

For an axial stress in an hourglass specimen, induced by thermal fatigue cycling, the radial or diametral strain can be expressed as (reference 3)

$$\epsilon_r = \alpha T - \mu (\sigma_z/E) - (\epsilon_z/2) \quad (1)$$

where

ϵ_r : radial or diametral strain
 α : coefficient of thermal expansion
 T : temperature
 μ : Poisson's ratio
 σ_z : axial stress
 E : Young's modulus
 ϵ_z : axial strain

In this study, the specimen was constrained with a pair of hydraulic grips, and so there was no axial strain or $\epsilon_z = 0$. Therefore, equation (1) can be simplified as

$$\epsilon_r = \alpha T - \mu(\sigma_z/E) \quad (2)$$

On the one hand, the radial or diametral strain ε_r can be measured with a diametral extensometer. That strain for the minimum radius R of the specimen is

$$\varepsilon_r = \Delta D / 2R \quad (3)$$

where

ΔD : diametral displacement

R : minimum radius of specimen

The axial stress σ_z can be measured with a load-cell above the specimen in the MTS machine. From Equations (2) and (3),

$$\Delta D / 2R = \alpha T - \mu(\sigma_z / E) \quad (4)$$

The $\Delta D / 2R$ and σ_z were measurable during the thermal fatigue cycling in this study. The validity of this equation was demonstrated by the measured $\Delta D / 2R$ and σ_z values, and the reported α , μ and E values (references 4 and 5) for the $T_{\max} = 1200$ and 1400°F , as shown in Table B-2.

VARIATION OF AXIAL STRESS AND DIAMETRAL STRAIN DURING THERMAL FATIGUE CYCLING

The measured minimum axial stress $(\sigma_z)_{\min}$, induced by simple thermal cycling or thermal and holding cycling was compressive. Its absolute value decreased (or became less compressive) with increasing number of cycle N and increasing maximum temperature T_{\max} , Figures A-4 and A-6. This behavior is similar to the stress relaxation of the specimen material, observed by some investigators during their studies on thermal and thermomechanical fatigue of structural alloys (reference 6). Such a stress relaxation is strongly temperature-dependent, and it occurs readily during the holding interval at elevated temperatures (reference 7).

Balandin (reference 8) reported that the increase of the maximum test temperature reduced the number of cycles before cracks develop. This was explained mainly by the increased thermal stresses on account of the larger temperature gradient. A considerable effect on the reduced resistance to thermal fatigue can be exerted also by a general lowering of the mechanical properties with increasing temperature, by accelerated creep and an increased coefficient of expansion.

The maximum diametral strain $(\varepsilon_r)_{\max}$ was measured to be nearly constant below 1550°F of the maximum temperature of the cycle T_{\max} , whereas it decreased with increasing time or number of thermal cycle at $T_{\max} = 1550^\circ\text{F}$ under simple thermal cycling, Figure A-5. On the one hand, it decreased with number of cycle at 1300°F or higher T_{\max} under thermal and holding cycling, Figure A-7.

COMPARISON OF MINIMUM AXIAL STRESSES FOR SIMPLE THERMAL CYCLING AND THERMAL AND HOLDING CYCLING

The minimum axial stresses $(\sigma_z)_{\min}$ for the simple thermal cycling and the thermal and holding cycling are compared in Figure A-8. At the five different maximum cycle temperatures T_{\max} , 1200, 1300, 1350, 1400, and 1550°F, and throughout the applied numbers of thermal cycle, the minimum axial stress is less compressive for the thermal and holding cycling than for the simple thermal cycling. This behavior is attributable to the holding at the maximum and minimum temperatures, during which presumably more microstructural degradation can occur.

MICROSTRUCTURAL CHANGE DURING THERMAL FATIGUE CYCLING

The microstructure was observed to change more with longer cycling and holding time and higher heating temperature, Figures A-9(b) and A-10. The microstructural change consisted of coarsening of intragrain precipitates γ' and γ'' , transformation of γ'' to δ phase, and formation of γ'' -depleted zone adjacent to grain boundaries. Such a microstructural change in alloy 718 was also observed by others (references 9-13). The zone without strengthening precipitate γ'' is weaker than the grain interior and unable to withstand high stresses. As the result, the zone is prone to cracking or intergranular cracking. The observed intergranular fracture, shown in Figure A-9(a), is believed to be attributed to the extension and interconnection of the intergranular cracks. Therefore, the controlling mechanism of thermal fatigue failure must be intergranular cracking. Glenn (references 14 and 15) and Franklin (reference 16) conducted studies on thermally fatigued Nimonic, and reported that above a maximum cycle temperature of 800°C intergranular fracture predominated but below this temperature transgranular fracture was usual.

On the basis of the above discussion, it is clear that the variations of $(\sigma_z)_{\min}$ and maximum diametral strain $(\epsilon_r)_{\max}$ are attributed to the microstructural degradation during the thermal cycling and thermal and holding cycling. Furthermore, the mechanism of thermal fatigue failure must be the intergranular cracking, arising from the microstructural degradation of the specimen material

The elongated and bowed grains and bent δ rods, shown in Figure A-10, evidence that the specimens crept under compression during the thermal and holding cycling of the constrained specimens.

THIS PAGE INTENTIONALLY LEFT BLANK

CONCLUSIONS

- The variation of the minimum axial stress and maximum diametral strain is attributed to the microstructural degradation during the simple thermal cycling and thermal and holding cycling.
- The mechanism of thermal fatigue failure is intergranular cracking, arising from the microstructural degradation of the specimen material.
- The microstructural degradation consists of growth of γ' and γ'' precipitates, phase transformation of γ'' to δ , and formation of γ'' -depleted zones along grain boundaries, which are prone to intergranular cracking.

RECOMMENDATION

- Investigate the thermomechanical fatigue behavior of DA718.

REFERENCES

1. J. F. Barker, D. D. Krueger, and D. R. Chang, "Advanced High Temperature Alloys: Processing and Properties," American Society for Metals, Metals Park, OH, 1986, pp. 125-137.
2. D. F. Paulonis, J. M. Oblak and D. S. Duvall, "Precipitation in Nickel-Base Alloy 718," Trans. ASM, Vol. 62, 1969, pp. 611-622.
3. A. E. Carden, "Thermal Fatigue – An Analysis of The Experimental Method," ORNL-TM-405, Oak Ridge National Laboratory, Operated by Union Carbide Corporation for the U. S. Atomic Energy Commission, 4 Jan 1963.
4. INCONEL alloy 718, Special Metals, www.specialmetals.com
5. INCONEL 718 Technical Data, High Temp Metals, <http://www.hightempmetals.com/techdata/hitempInconel718data.php>
6. Huseyin Sehitoglu, "Thermal and Thermomechanical Fatigue of Structural Alloys," ASM Handbook, vol. 19, ASM International, Materials Park, OH, 1997, pp. 527-556.
7. L. F. Coffin, Jr., "Strain Cycling and Thermal Stress Fatigue," Presented at the Fourth Sagamore Ordnance Materials Research Conference, Racquette Lake, New York, 21-23 Aug 1957.
8. Yu. F. Balandin, "Thermal Fatigue of Metals," Material Science and Heat Treatment of Metals, vol. 3, No. 3-4, 1 Mar 1961, pp. 91-96.
9. J. F. Radavich and B. H. Lawless, "Effect of Thermal Exposure on Microstructural Evolution in Alloy 718 Fasteners," in Superalloys 718, 625, 706 and Various Derivatives, Edited by E. A. Loria, TMS (The Minerals, Metals and Materials Society), 2001, pp. 433-442.
10. W. D. Cao and R. L. Kennedy, "Thermal Stability of Alloys 718 and Allvac 718- ER," in Superalloys 718, 625, 706 and Various Derivatives, Edited by E. A. Loria, TMS (The Minerals, Metals and Materials Society), 2001, pp. 455-464.
11. W. D. Cao and R. L. Kennedy, "Improving Stress Rupture Life of Alloy 718 by Optimizing Al, Ti, P and B Contents," in Superalloys 718, 625, 706 and Various Derivatives, Edited by E. A. Loria, TMS (The Minerals, Metals and Materials Society), 2001, pp. 477-488.
12. A. K. Koul, P. Au, N. Bellinger, R. Thamburaj, W. Wallace and J-P. Immarigeon, "Development of a Damage Tolerant Microstructure for Inconel 718 Turbine Disc Material," in Superalloys 1988, Edited by S. Reichman, D. N. Duhl, G. Maurer, S. Antolovich and C. Lund, The Metallurgical Society, 1988, pp. 3-12).

13. J. F. Radavich, "The Physical Metallurgy of Cast and Wrought Alloy 718," in Superalloy 718 – Metallurgy and Applications, Edited by E. A. Loria, The Minerals, Metals and Materials Society, 1989, pp. 229-240.
14. E. Glenny, J. E. Northwood, S. W. K. Shaw and T. A. Taylor, J. Inst. Metals, Vol. 87, 1958-59, p. 294.
15. E. Glenny and T. A. Taylor, J. Inst. Metals, Vol. 88, 1959-60, p. 449.
16. A. W. Franklin, J. Heslop, and R. A. Smith, J. inst. Metals, Vol. 92, 1963-64, p. 313.

APPENDIX A LIST OF FIGURES

| <u>Figure</u> | <u>Title</u> | <u>Page No.</u> |
|---------------|---|-----------------|
| A-1 | Scanning Electron Micrograph of Super Alloy Inconel 718 | 14 |
| A-2 | Apparatus for Thermal Fatigue Test | 14 |
| A-3(a) | Simple Thermal Cycle | 15 |
| A-3(b) | Thermal and Holding Cycle | 15 |
| A-4 | Variation of Minimum Axial Stress with Number of Simple Thermal Cycle | 16 |
| A-5 | Variation of Maximum Diametral Strain with Number of Simple Thermal Cycle | 16 |
| A-6 | Variation of Minimum Axial Stress with Number of Thermal and Holding Cycle | 17 |
| A-7 | Variation of Maximum Diametral Strain with Number of Thermal and Holding Cycle | 17 |
| A-8 | Variation of Minimum Axial Stress under Simple Thermal Cycling and Thermal and Holding Cycling (*1200: Simple Thermal Cycling at Max. Temp. 1200°F, 1200X: Thermal and Holding Cycle under Max. Temp. 1200°F) | 18 |
| A-9(a) | Intergranular Fracture of Specimen, Subjected to Simple Thermal Cycling of 600-1350°F | 18 |
| A-9(b) | Intergranular Cracking in a Specimen, Subjected to Simple Thermal Cycling of 600-1400°F | 19 |
| A-10 | Elongated Grains, and Bowed or Bent δ Rods within and along Grain Boundaries in Specimen, Subjected to Thermal and Holding Cycling at 600-1500°F | 19 |
| A-11 | SEM Fractographs of Specimen, Subjected to Simple Thermal Cycling of 660-1550°F | 20 |
| A-12 | SEM Fractographs of Specimen, Subjected to Thermal and Holding Cycling of 600-1400°F | 20 |

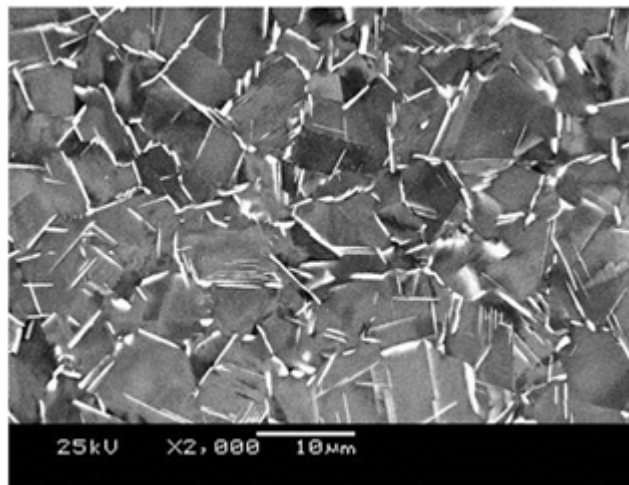


Figure A-1: Scanning Electron Micrograph of Super Alloy Inconel 718



Figure A-2: Apparatus for Thermal Fatigue Testing

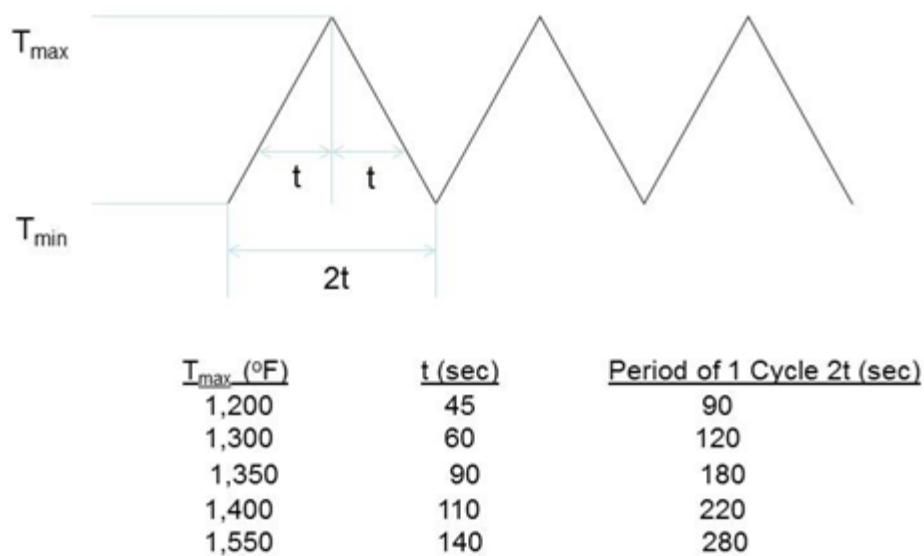


Figure A-3(a): Simple Thermal Cycle

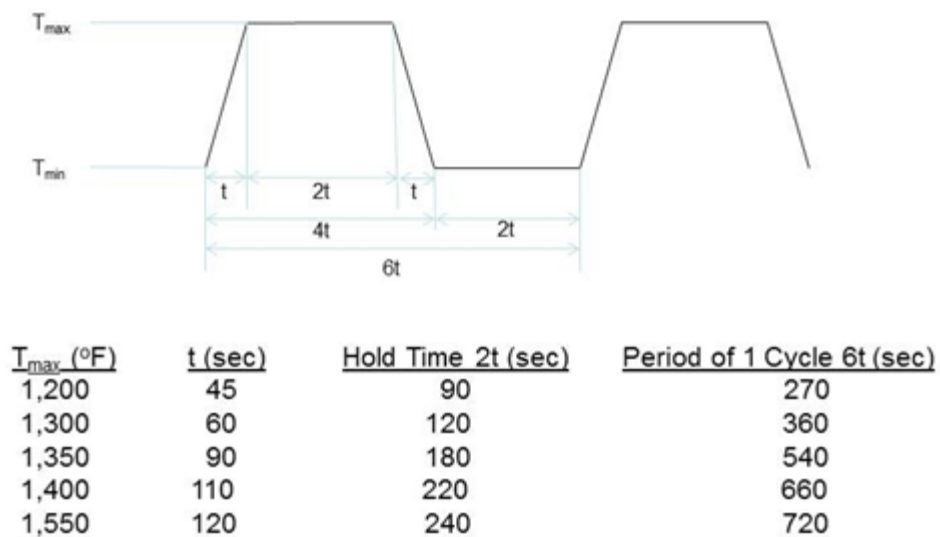


Figure A-3(b): Thermal and Holding Cycle

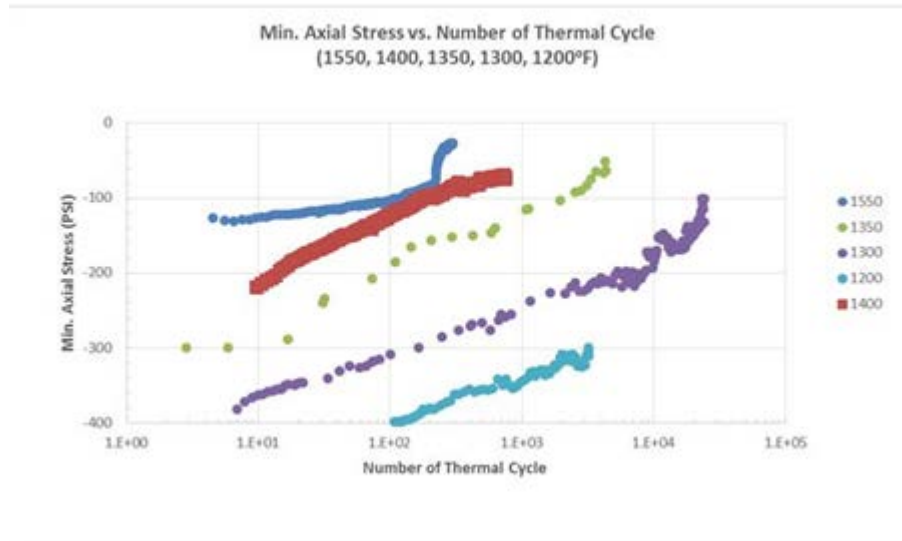


Figure A-4: Variation of Minimum Axial Stress with Number of Simple Thermal Cycle

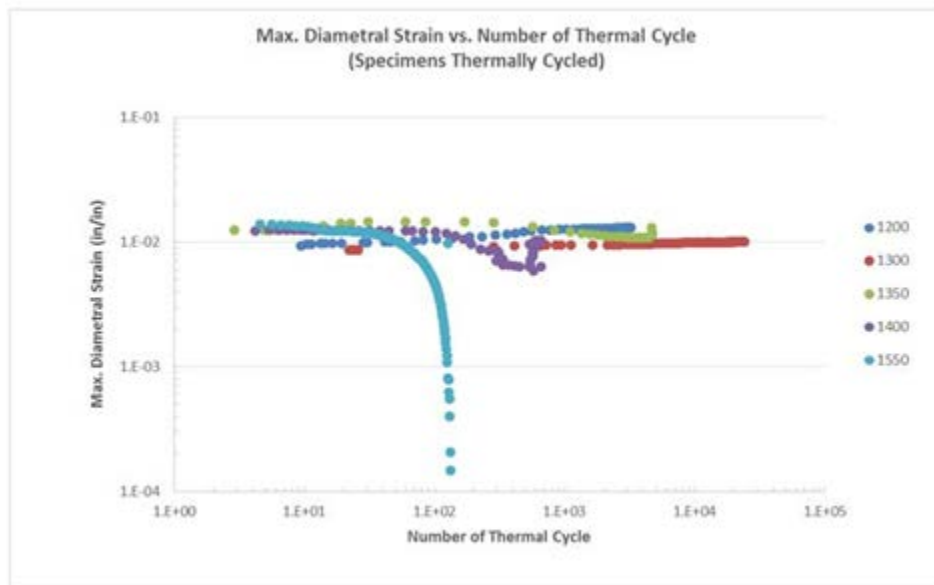


Figure A-5: Variation of Maximum Diametral Strain with Number of Simple Thermal Cycle

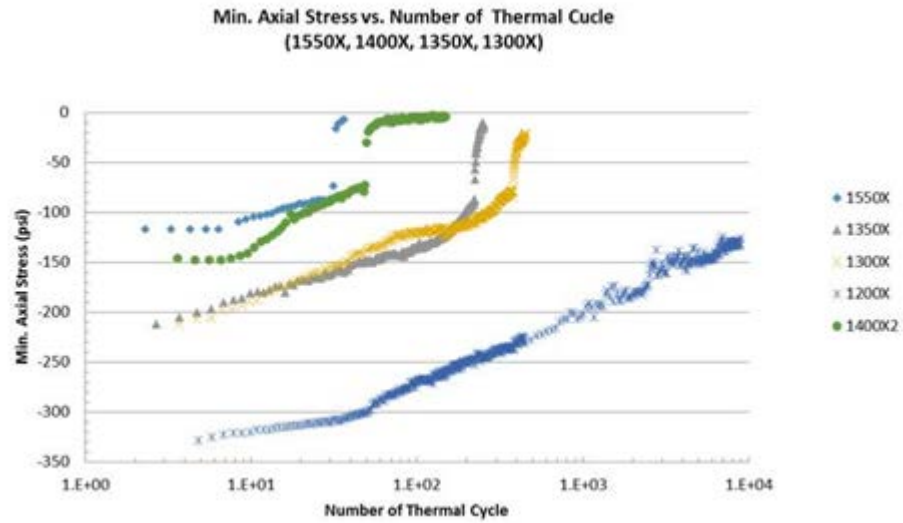


Figure A-6: Variation of Minimum Axial Stress with Number of Thermal and Holding Cycle

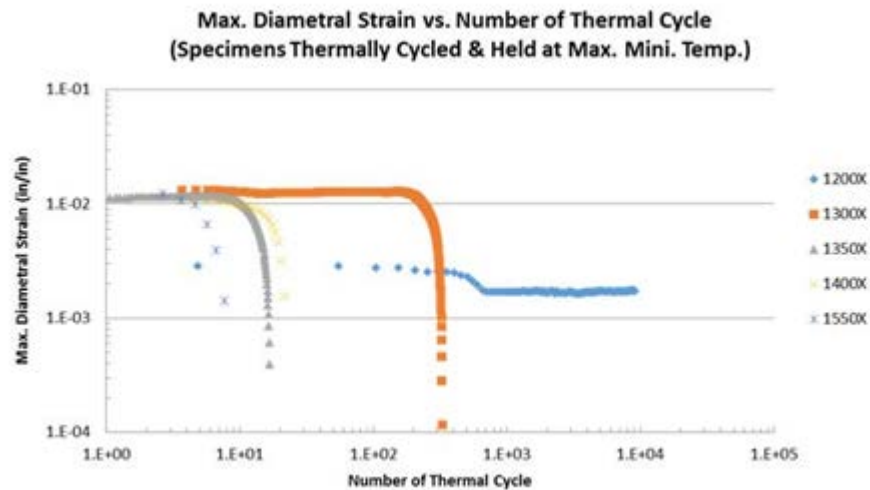


Figure A-7: Variation of Maximum Diametral Strain with Number of Thermal and Holding Cycle

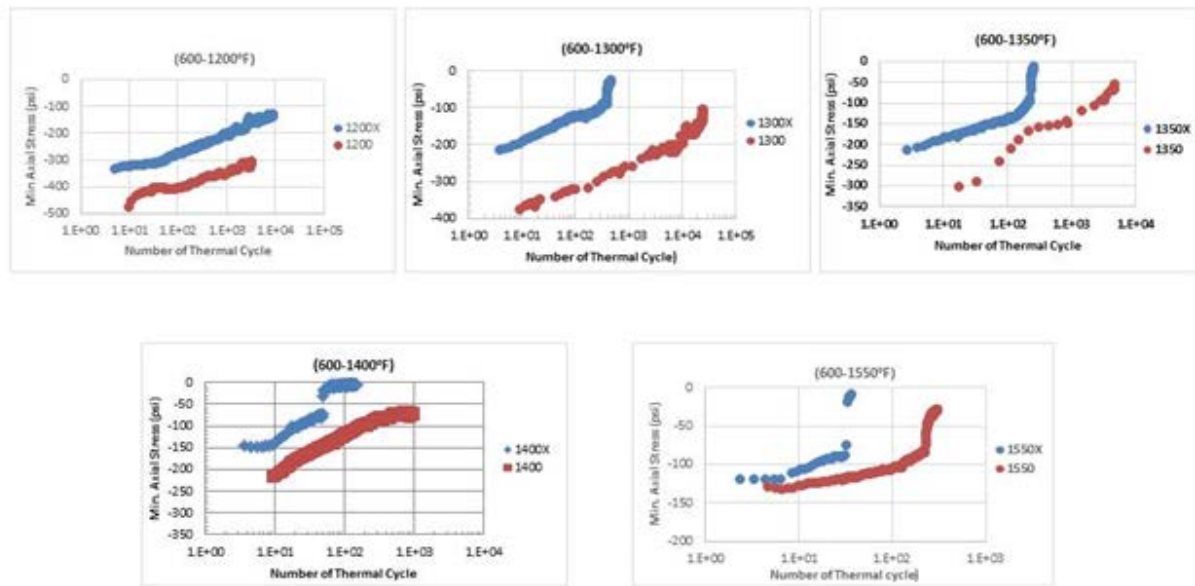


Figure A-8: Variation of Minimum Axial Stress under Simple Thermal Cycling and Thermal and Holding Cycling (*1200: Simple Thermal Cycling at Max. Temp 1200°F; 1200X: Thermal and Holding cycle under Max. Temp 1200°F)

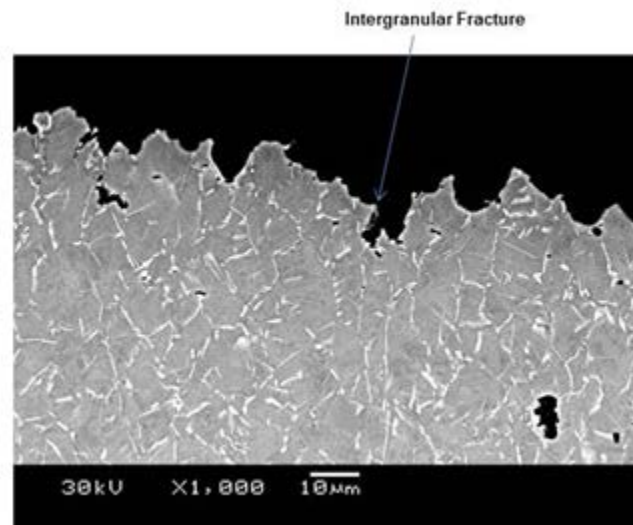
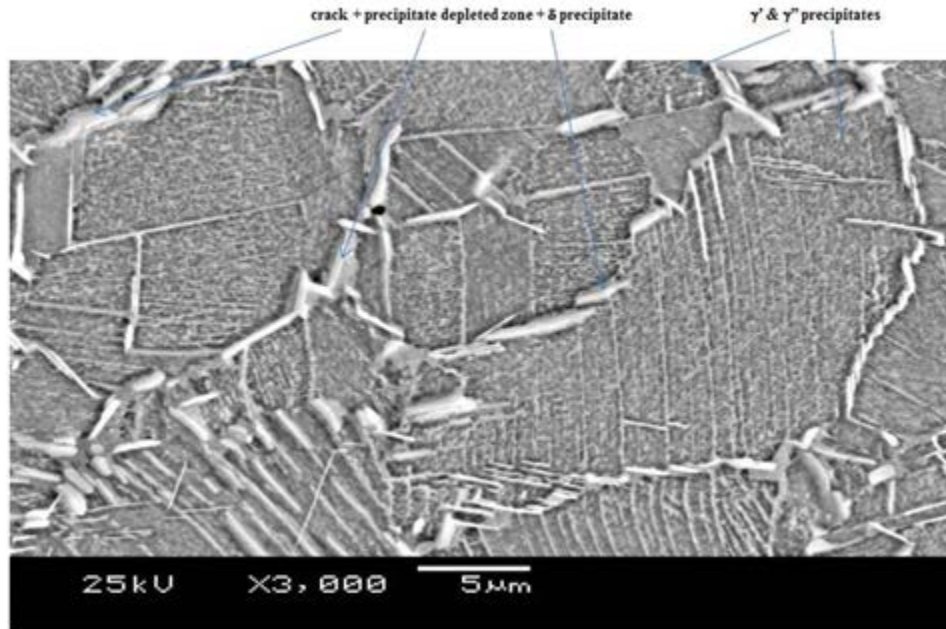


Figure A-9(a): Intergranular Fracture in Specimen, Subjected to Simple Thermal Cycling of 600-1350°F



Thermal A-9(b): Intergranular Cracking in Specimen, Subjected to Simple Thermal Cycling of 600-1400°F

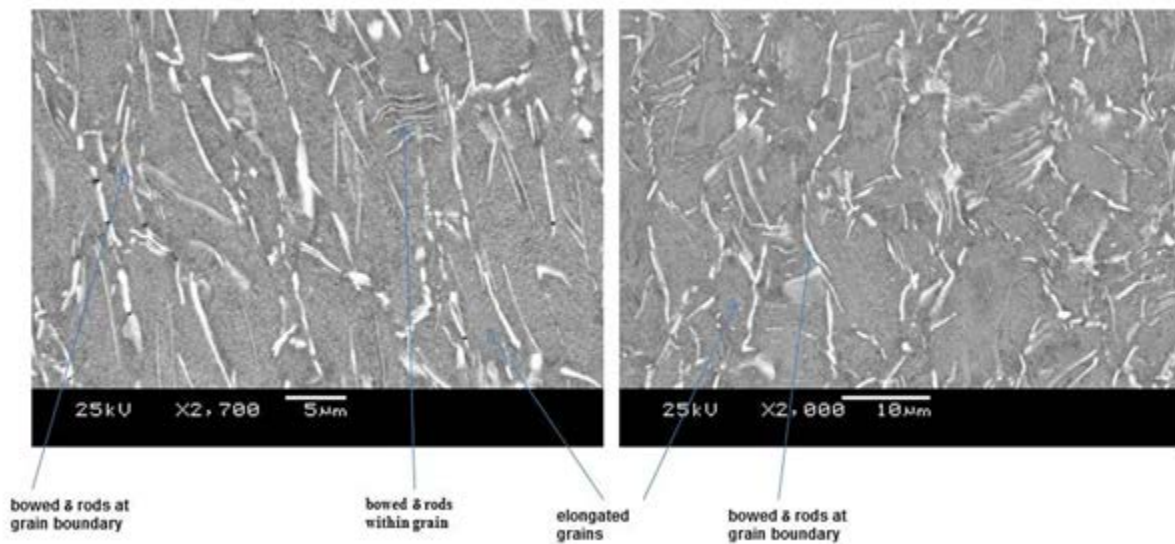


Figure A-10: Elongated Grains, and Bowed or Bent δ Rods within and along Grain Boundaries in Specimen, Subjected to Thermal and Holding Cycling at 600-1500°F

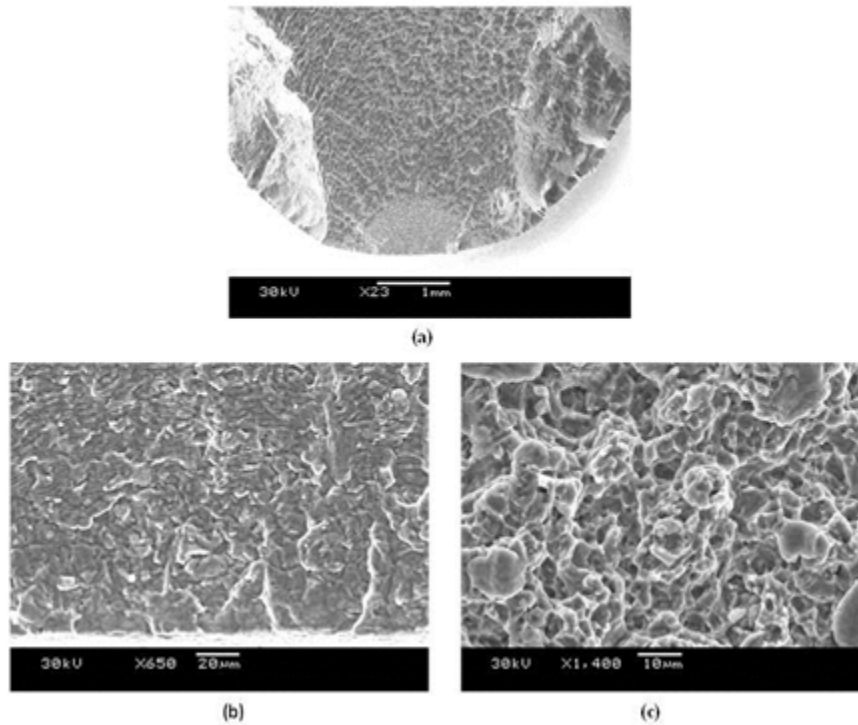


Figure A-11: SEM Fractographs of Specimen, Subjected to Simple Thermal Cycling of 600-1550°F

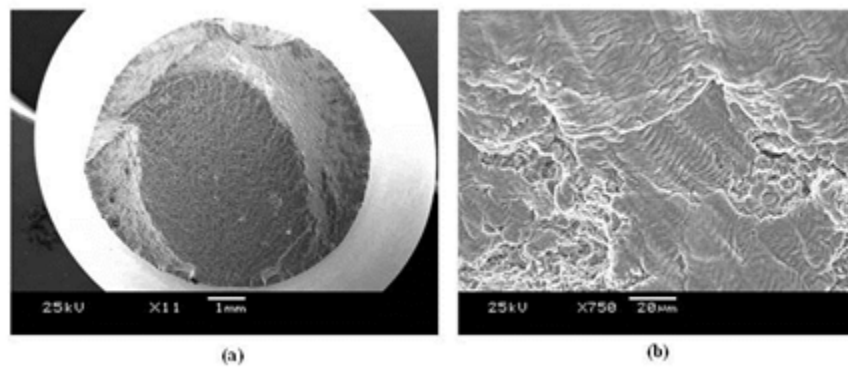


Figure A-12: SEM Fractographs of Specimen, Subjected to Thermal and Holding Cycling of 600-1400°F

APPENDIX B TABLES

Table B-1: Chemical Composition (wt %) of Super Alloy Inconel 718

| | | | |
|----|-----------|----|-------------|
| Al | 0.2 – 0.8 | Mo | 2.8 -3.3 |
| B | 0.006 max | Ni | 50 - 55 |
| C | 0.08 max | Nb | 4.75 – 5.5 |
| Cr | 17 -21 | P | 0.015 max |
| Co | 1 max | Si | 0.35 max |
| Cu | 0.3 max | S | 0.015 max |
| Fe | Balance | Ti | 0.65 – 1.15 |
| Mn | 0.35 max | | |

Table B-2: Validation of Thermal Stress and Strain Relationship $\Delta D/2R = \alpha T - \mu(\sigma_z/E)$

| T | α | αT | E | σ_z | μ | $\mu\sigma_z$ | $\mu\sigma_z/E$ | $[\alpha T - (\mu\sigma_z/E)]$ | | $\Delta D/2R$ |
|------|----------|------------------------|--------------------------------|---------------|------------------------------|------------------|------------------|--------------------------------|---------|---------------|
| | | ($^{\circ}\text{F}$) | ($10^{-6}/^{\circ}\text{F}$) | (10^{-2}) | ($\text{psi} \times 10^3$) | (psi) | (psi) | (10^{-3}) | | |
| 1200 | 8.4 | 1.008 | 23.7 | -400 | 0.283 | -113.2 | -4.776 | 0.0149 | \cong | 0.01303 |
| 1400 | 8.9 | 1.246 | 22.3 | -120 | 0.306 | -36.7 | -1.646 | 0.0141 | \cong | 0.01216 |

THIS PAGE INTENTIONALLY LEFT BLANK

DISTRIBUTION:

Office of Naval Research (Code 35/William Nickerson)
875 N. Randolph St., Room 1143B, Arlington, VA 22203
William.nickerson@navy.mil
NAVAIRSYSCOM (AIR-4.0T/Dr. James Sheehy), Bldg. 2109, Room N122
48150 Shaw Road, Patuxent River, MD 20670
James.sheehy@navy.mil
NAVAIRSYSCOM (AIR-4.0T/Ms. Kristi Wiegman), Bldg. 2109
48150 Shaw Road, Patuxent River, MD 20670
Kristi.wiegman@navy.mil
NAVAIRSYSCOM (AIR-4.3), Bldg. 2187, Suite 3340
48110 Shaw Road, Patuxent River, MD 20670-1906
Colleen.deal@navy.mil
NAVAIRSYSCOM (AIR-4.3T/Jerry Rubinsky), Bldg. 2187, Suite 3322
48110 Shaw Road, Patuxent River, MD 20670-1906
Jerry.rubinsky@navy.mil
NAVAIRSYSCOM (AIR-4.3.4/Darrel Tenney), Bldg. 2188
48066 Shaw Road, Patuxent River, MD 20670-1908
Darrel.tenney@navy.mil
NAVAIRSYSCOM (AIR-4.3.4.1/Robert Kowalik), Bldg. 2188
48066 Shaw Road, Patuxent River, MD 20670-1908
Robert.kowalik@navy.mil
FRC/ISSC Jacksonville (AIR-4.3.4.6/John Benfer)
Naval Air Station, Jacksonville, FL 32212
John.benfer@navy.mil
DTIC, 8725 John J. Kingman Road, Suite 0944, Ft. Belvoir, VA 22060-6218

FOR OFFICIAL USE ONLY

FOR OFFICIAL USE ONLY